

# ZnO nanowires as photocatalyst for H<sub>2</sub> production from ethanol<sub>(aq)</sub> in gas phase

Narcís Homs<sup>1,2,\*</sup>, Alberto C. Sola<sup>1</sup>, Paulina R. Martínez-Alanis<sup>1,2</sup>, Xavier Alcobé<sup>3</sup>, Frank Güell<sup>4</sup>, Pilar Ramírez de la Piscina<sup>1,\*</sup>

*<sup>1</sup>Departament de Química Inorgànica i Orgànica, secció de Química Inorgànica and Institute of Nanoscience and Nanotechnology (IN2UB), Universitat de Barcelona, Martí i Franquès 1, 08028 Barcelona, Spain*

*<sup>2</sup>Catalonia Institute for Energy Research (IREC), Jardins de les Dones de Negre 1, 08930 Barcelona, Spain*

*<sup>3</sup>Scientific and Technological Centers (CCiTUB), Lluís Solé i Sabarís 1-3, 08028 Barcelona, Spain*

*<sup>4</sup>ENPHOCAMAT Group, Institute of Nanoscience and Nanotechnology (IN2UB), Universitat de Barcelona, Martí i Franquès 1, 08028 Barcelona, Spain.*

\*Corresponding authors:

Narcís Homs, [narcis.homs@qi.ub.edu](mailto:narcis.homs@qi.ub.edu); Pilar Ramírez de la Piscina, [pilar.piscina@qi.ub.edu](mailto:pilar.piscina@qi.ub.edu)

## **Abstract**

ZnO nanowires (NWs) with wurzite structure and a very high [0001] preferred orientation, were grown on a ZnO thin film using a catalyst-free vapor-solid process. ZnO NWs were characterized by FESEM, XRD, HRTEM, XPS, PL and Raman spectroscopy and used as photocatalysts for the transformation of ethanol<sub>(aq)</sub> in the gas phase. The presence of different defects such as oxygen vacancies was evidenced. The photocatalytic process was followed by *in-situ* diffuse reflectance infrared spectroscopy (DRIFTS) coupled to on-line mass spectrometry (MS) analysis. The surface species determined during the irradiation ( $\lambda=365$  nm) of ZnO NWs under ethanol/water vapor flow at room temperature are related with the hydrogen production and carbon-containing products evolved.

**Keywords:** ZnO nanowires; photocatalytic H<sub>2</sub>; H<sub>2</sub> from ethanol<sub>(aq)</sub>; ZnO photocatalyst; *in-situ* DRIFTS.

## Introduction

The photocatalytic behavior of nanostructured semiconductor metal oxides depends on their structure, morphology, surface area and surface defects [1-9]. ZnO is an interesting semiconductor which has attracted increased attention as photocatalyst in the last years. Its band gap energy (3.3 eV) is similar to that of TiO<sub>2</sub> and shows a high exciton binding energy, 60 meV [10]. Besides a high photosensitivity, environmentally friendly nature and low cost, ZnO shows a high surface reactivity because of its large number of active surface defect states [11]. Several efforts have been done to enhance the photocatalytic activity of ZnO by tailoring its morphology, particle size, and concentration of oxygen defects, surface facets and surface area [4]. DFT calculations have shown that exposed polar surfaces play a main role in the stability of holes upon light excitation and in the organic compound decomposition [3]. On the other hand, nonpolar surfaces have been proposed more appropriate for photoreduction processes [3].

1D-, 2D- and 3D-nanostructured ZnO has been prepared with different morphologies such as nanorods, nanowires, nanotubes, nanosheets and nanoflowers [11], among them, 1D nanostructures are considered good candidates as photocatalysts because, among other reasons, their surface-to-volume ratio [12]. Moreover, the delocalization of electrons in 1D nanostructures favors the separation of photogenerated charge carriers improving the efficiency of photocatalysts. Most of the uses of nanostructured ZnO in photocatalysis have been related with the photodegradation of contaminants such as volatile organic compounds and dyes for environmental pollution control and in the water treatment [13]. However, ZnO could be also considered a good candidate

for the photocatalytic H<sub>2</sub> production from alcoholic solutions. Specifically, the use of ethanol as a sacrificial agent could provide a good opportunity for the hydrogen production from a renewable source. This process has been largely studied over TiO<sub>2</sub>-based systems but there is a lack of papers related with the use of solely ZnO as photocatalyst for H<sub>2</sub> evolution [14,15,16].

Some of us have reported the preparation of ZnO 1D nanowires (ZnO NWs) using a catalyst-free vapor-transport method [17]. This background led us to study the photocatalytic H<sub>2</sub> evolution using ethanol<sub>(aq)</sub> in gas phase at room temperature over pristine ZnO NWs without any dopant. The characterization of the ZnO NWs, including the determination of different defects, was carried out using field emission scanning electron microscopy (FESEM), X-ray diffraction (XRD), high-resolution transmission electron microscopy (HRTEM), X-ray photoelectron spectroscopy (XPS), and photoluminescence (PL) and Raman spectroscopy. The photocatalytic process was followed by *in-situ* diffuse reflectance infrared spectroscopy (DRIFTS) coupled to on-line mass spectrometry (MS) analysis. This allowed the determination of several surface species generated during the photocatalytic process, which are related with the products formed. The post-reaction ZnO NWs were analyzed by FESEM, XRD, XPS and PL and Raman spectroscopy.

## **Experimental**

ZnO NWs were grown on a ZnO thin film deposited on a Si (001) single crystal by radio frequency reactive sputtering (13.56 MHz, 85 W) using a polycrystalline zinc target of 99.99% purity and Ar/O<sub>2</sub>=10 molar ratio. The final thickness of the ZnO film was about 150 nm. A catalyst-free vapor-solid process was used to

grow the ZnO NWs on the ZnO film. ZnO and graphite powders (1:1 mole ratio) were mixed and placed close to the ZnO film in a horizontal quartz tube, which was inside a furnace. The system was heated up to 900 °C, kept at 900 °C for 30 min, and then cooled down to room temperature; the process was done under Ar flow (400 mL min<sup>-1</sup>) at atmospheric pressure [17].

FESEM was performed using a JEOL JSM-7100F operated at 15 kV. XRD measurements were performed in a PANalytical X'Pert PRO MPD alpha1 powder diffractometer, in Bragg-Brentano reflection geometry, with Cu K $\alpha$ 1 radiation ( $\lambda=1.5406$  Å) selected by means of a curved Johansson type primary monochromator and with an 1D silicon strip X'Celerator detector (active length 2.122 °). The final useful scans were  $2\theta/\omega$  ( $\omega$ - $\theta$ =-2) from 10 to 65° 2 $\theta$ , step size 0.017° 2 $\theta$ , and 2000 seconds per step (15 hours of total measuring time per scan). HRTEM was performed with a JEOL 2010F microscope equipped with a field emission gun and operated at 200 kV; NWs were mechanically removed from the substrate and deposited over carbon-coated copper grids.

XPS measurements have been performed using a PHI 5500 Multitechnique System equipped with a monochromatic X-ray radiation source of Al K $\alpha$  (1486.6 eV) and 350 W. The sample was placed perpendicular to the analyzer axis and calibrated using the 3d<sub>5/2</sub> line of Ag with a full width at half maximum (FWHM) of 0.8 eV. The analyzed area was a circle of 0.8 mm diameter and the resolution for the spectra was 187.5 eV of Pass Energy and 0.8 eV/step for the general spectra and 23.5 eV of Pass Energy and 0.1 eV/step for the depth profile spectra. All measurements were made in an ultra-high vacuum (UHV) chamber pressure between 5·10<sup>-9</sup> and 2·10<sup>-8</sup> torr. The BE values were referred to the BE of the C 1s of the adventitious carbon at 284.8 eV.

Room-temperature PL spectra were recorded with a chopped Kimmon IK Series He-Cd laser (325 nm and 40 mW). Fluorescence was dispersed through a SpectraPro 2750 (focal length 750 mm) f/9.8 monochromator, detected with a Hamamatsu H8259-02 photomultiplier, and amplified through a Stanford Research Systems SR830 DSP Lock-in amplifier. A 360 nm filter was used to filtering the stray light. All spectra were corrected for the response function of the setups. Raman measurements were made with a Jobin Yvon LabRAM HR800 spectrometer exciting at a wavelength of 325 nm.

The *in-situ* DRIFTS-MS photocatalytic reaction was carried out using a FTIR spectrophotometer Bruker Vertex 70 in DRIFTS mode, coupled to a mass spectrometer ThermoStar GSD320T1. The samples were deposited into a Harrick Scientific DRIFTS cell chamber with quartz and ZnSe windows and irradiated with a Hamamatsu Lightning Cure lamp ( $\lambda=365$  nm,  $20$  mW  $\text{cm}^{-2}$ ). The catalysts were irradiated at  $28$  °C under a He flow saturated with ethanol/water vapor=1/9.6 (mol/mol), a gas mixture composition close to that of bioethanol. During irradiation, DRIFT and mass spectra were recorded as a function of time; 256 scans at a resolution of  $4$   $\text{cm}^{-1}$  were used to register the DRIFT spectra. The  $m/z$  fragments corresponding to  $\text{CH}_3\text{CH}_2\text{OH}$ ,  $\text{CH}_3\text{CHO}$ ,  $\text{CH}_3\text{COOH}$ ,  $\text{CH}_3\text{COCH}_3$ ,  $\text{CH}_4$ ,  $\text{CO}_2$ ,  $\text{CO}$  and  $\text{H}_2$  were continuously analyzed by MS. The corresponding experiments under dark conditions, the blank cell test and that using the reference ZnO thin film as photocatalyst, were also carried out.

## **Results and Discussion**

### **Characterization of ZnO NWs**

As stated in the experimental section, ZnO NWs were prepared using a ZnO thin film as seed layer deposited over a Si (001) single crystal [17]. The morphology of the ZnO NWs was determined by FESEM (Figure 1a). An uniform and dense array of ZnO NWs with average diameter of 50 nm, length of about 0.5  $\mu\text{m}$ , and density between 40-80 NW  $\mu\text{m}^{-2}$  was obtained. A specific surface area in the range of 15-30  $\text{m}^2 \text{g}^{-1}$  was calculated using the FESEM average dimensions and assuming a cylindrical shape.

XRD pattern of ZnO NWs (Figure 2A) revealed the presence of mainly wurtzite ZnO (space group  $P6_3mc$ , JCPDS 00-036-1451), with cell parameters  $a \approx 3.25 \text{ \AA}$  and  $c \approx 5.20 \text{ \AA}$ , with very high [0001] preferred orientation and significant anisotropic peak enlargement. The 002 diffraction peak is splitted indicating that very probably there are two main different ZnO (0001) domains. Besides the peaks characteristic of the ZnO wurtzite phase, Figure 2A shows other peaks with very low intensity, these peaks can be related with the presence of two polymorphic phases of  $\text{Zn}_2\text{SiO}_4$  (JCPDS 04-008-2034 and 01-078-5360). In order to investigate the formation of  $\text{Zn}_2\text{SiO}_4$ , the initial ZnO thin film deposited over Si (001) single crystal, which was used as seed layer for growing the ZnO nanowires, was heated at 900  $^\circ\text{C}$  which was the temperature used for the nanowire growing. XRD pattern of the sample after the treatment (not shown) showed peaks characteristic of the above indicated  $\text{Zn}_2\text{SiO}_4$  crystalline phases (JCPDS 04-008-2034 and 01-078-5360), meanwhile peaks related with the presence of ZnO were not found. These results indicated that residual  $\text{Zn}_2\text{SiO}_4$  could be formed in the interface Si/ZnO-film during the preparation of ZnO NWs according with the XRD results discussed above and previous annealing studies of ZnO films on silicon [18].

For a deeper structural characterization of ZnO NWs, HRTEM analysis was performed (Figure 2B). According with XRD results, HRTEM analysis confirmed that ZnO NWs crystallize in the typical wurtzite structure and that ZnO NWs grow along the [0001] direction. Figure 2B shows a single ZnO NW visualized in the [-1100] direction. The Fourier transform image (inset in Figure 2B) also accords with the only presence of several planes of wurtzite ZnO.

The ZnO NWs were characterized by XPS (Figure 3). The analysis of O 1s core level spectrum has been previously used for the identification of several surface defects on ZnO [5,19]; for ZnO NWs, an increase in the amount of surface defects have been found when the aspect ratio of the NWs increased [20]. The registered spectrum corresponding to O 1s (Figure 3a) is rather complex and can be deconvoluted into three components, the main broad component at 532 eV can be related with surface OH associated with surface defects and/or surface O<sup>2-</sup> in oxygen-deficient regions [2,5,7]. The O 1s component centered at 530.1 eV is related with lattice O<sup>2-</sup> and the very small component at 533.3 eV with chemisorbed oxygen species [2,5,7].

On the other hand, the Zn 2p<sub>3/2</sub> core level showed a peak characteristic of Zn<sup>2+</sup> in ZnO with maximum at 1022 eV, and for the C 1s peak, besides the corresponding adventitious carbon signal at about 284.4 eV, a low intensity peak at 288-290 eV was observed (spectra not shown), which can be assigned to the presence of carbonate species [21]; carbonate species could be formed from CO<sub>2</sub> during the preparation of ZnO NWs.

Figure 4A shows the room-temperature PL emission spectrum of ZnO NWs, which show emissions in both the UV and visible spectral regions. The emission peak at 377 nm (3.29 eV) corresponds to the near band-edge emission,



associated with exciton recombination processes [22]. The broad emission band observed in the visible range (430-830 nm) with maximum at around 650 nm (1.9 eV) can be attributed to the presence of different defects [23,24]. Although it is not possible to unambiguously assign this band, its broadness can be related with the presence of defects with different characteristics: interstitials ( $Zn_i$  and  $O_i$ ) and vacancies ( $V_{Zn}$  and  $V_O$ ) [25]. However, other defects such as “antisites” ( $Zn_O$  and  $O_{Zn}$ ), chemisorbed  $O_2$  or more complex defects can also contribute to the mentioned broad emission band [26].

The Raman spectrum of the ZnO NWs (Figure 4B) shows a wide band of low intensity at 400-500  $cm^{-1}$  corresponding to the  $E_2$  mode and a main well-defined band at about 580  $cm^{-1}$ , which is related with the  $E_1(LO)$  mode and associated with oxygen deficiency [27,28].

### **Photocatalytic reaction**

The photocatalytic transformation of ethanol<sub>(aq)</sub> in gas phase over ZnO NWs was followed by *in-situ* DRIFTS-MS. As stated in the experimental section, the sample was irradiated under a He flow saturated with 1/9.6 (mol/mol) ethanol/water vapor at room temperature. During irradiation, DRIFT and mass spectra were recorded *in-situ* as a function of time; these results are shown in Figure 5.

Figure 5A shows the analysis of the MS profiles of main products evolved during the *in-situ* irradiation process under continuous flowing of the ethanol/water vapor. Besides  $H_2$ , CO,  $CH_4$ ,  $CO_2$  and acetaldehyde were the main products; acetic acid and acetone were also detected. After switch off the irradiation, all products rapidly decreased in the outlet flow. The experiments

carried out without illumination, and the blank cell test without photocatalyst did not give any detectable product from ethanol transformation.

Figure 5B shows the DRIFT spectrum registered in the 1800-1300  $\text{cm}^{-1}$  region during the *in-situ* irradiation process under continuous flowing of the ethanol/water vapor flow (spectrum a). The band at 1742  $\text{cm}^{-1}$  can be related with the presence of acetaldehyde ( $\nu(\text{C}=\text{O})$ ). Although the bands below 1650  $\text{cm}^{-1}$  can be reasonably attributed to the presence of different surface carboxylate and carbonate species, the poor definition of the spectrum makes difficult a straightforward assignment of these bands.

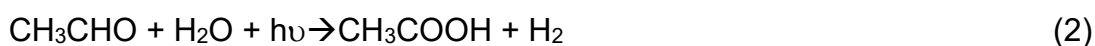
Spectrum b in Figure 5B was obtained after the reaction-quenching by switching off the light and stop the reactants flow. The bands centered at 1543  $\text{cm}^{-1}$  and 1515  $\text{cm}^{-1}$ , and 1385  $\text{cm}^{-1}$  and about 1312  $\text{cm}^{-1}$  can be related with the corresponding  $\nu_{\text{as}}(\text{COO})$  and  $\nu_{\text{s}}(\text{COO})$  modes of different acetate adsorbed species [29,30]. Moreover, the contribution of different components to the very broad band centered at 1385  $\text{cm}^{-1}$  can be proposed. Formate species over ZnO have been related with bands at 1385-1380  $\text{cm}^{-1}$  ( $\delta(\text{CH})$ ) and at about 1610  $\text{cm}^{-1}$  ( $\nu_{\text{as}}(\text{COO})$ ) [31-34]. Moreover, the  $\nu_3$  of free  $\text{CO}_3^{2-}$  ion is expected about 1440  $\text{cm}^{-1}$ , and, other surface carbonate species could contribute to the broadness of the bands at 1543  $\text{cm}^{-1}$  and 1515  $\text{cm}^{-1}$ .

On the other hand, a definite band centered at 1647  $\text{cm}^{-1}$  has been related to the  $\nu(\text{C}=\text{O})$  of aldehyde species such as formaldehyde and/or unsaturated aldehydes [35-37]. Finally, it is worth of mention that in the quenching process (spectrum b in Figure 5B), a band at 1688  $\text{cm}^{-1}$  is clearly visible; this band can be attributed to the presence of surface acyl species [30,38,39], which could be the precursors of the surface carboxylate species detected.

Taking into account the results exposed above, and on the basis of previous studies on ethanol interactions with ZnO-based catalysts and photo-reforming of ethanol aqueous solutions over TiO<sub>2</sub>-based samples [14,30,40-42], we propose several processes that could take place over ZnO NWs during the irradiation of an ethanol/water vapor flow at room temperature. The first step could be the photocatalytic transformation of ethanol into acetaldehyde and H<sub>2</sub>.



This could proceed by direct ethanol oxidation or via previous ethoxide formation and its further oxidation. The observed CH<sub>3</sub>COOH evolution can result from CH<sub>3</sub>CHO and H<sub>2</sub>O with H<sub>2</sub> evolution under irradiation:



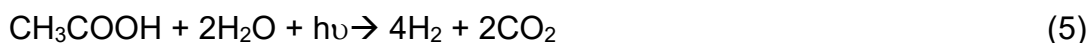
Although the presence of CH<sub>4</sub> can be mainly related with the decomposition of CH<sub>3</sub>CHO under irradiation:



CH<sub>4</sub> can be also obtained from the corresponding CH<sub>3</sub>COOH decomposition:



Moreover, acetic acid could be also photo-reformed to further produce H<sub>2</sub> and CO<sub>2</sub>:



On the other hand, the decomposition of ethanol to acetone over ZnO-based catalysts has been described as a series of successive reactions such as dehydrogenation and aldol condensation over basic centers [30,43].

After the *in-situ* DRIFTS-MS photocatalytic reaction, the ZnO NWs were analyzed by FESEM, XRD, XPS, PL and Raman spectroscopy. No significant changes in the ZnO NWs were observed in morphology, structure and surface

characteristics as determined by FESEM, XRD and XPS analysis. Figure 1b shows the corresponding image of the post-reaction ZnO NWs sample. Only slight displacements or folding of the uniform nanowire disposition were observed after the contact with the flow of ethanol<sub>(aq)</sub> vapor under irradiation. Figure 3b shows the XP spectrum of the O 1s core level analysis of the post-reaction ZnO NWs sample. As can be seen, the ratio of the O<sup>2-</sup> lattice species (peak about 530.1 eV) with respect to those associated with OH and/or surface defects (peak about 532 eV) decreases; the presence of abundant adsorbed species remaining after the photocatalytic test could contribute to this.

On the other hand, Figure 4A and 4B show the PL emission and Raman spectra, respectively, of the post-reaction ZnO NWs. Slight differences in the position and broadness of the visible emission band (Figure 4A) can be observed. Moreover, the exciton peak is located at 378 and 376 nm and the full width at half maximum (FWHM) are around 105 and 91 meV, for the fresh and the post-reaction photocatalysts, respectively. It has been proposed that defects are the origin of this shift by slightly modifying the energy band structure of ZnO, and the broadening observed on the FWHM indicates that the quantity of intrinsic defects could be higher for the fresh sample [44].

In the same line, some differences can be also observed in the Raman E<sub>1</sub>(LO) mode when comparing the phonon frequencies and the FWHM of the peak at around 580 cm<sup>-1</sup> for the fresh and the post-reaction samples (Figure 4B). The used photocatalyst reaction exhibits a small blue shift (1.4 cm<sup>-1</sup>) and a decrease of the mode line width (FWHM by 1 cm<sup>-1</sup>) when compared to the fresh sample. Existence of defects would result in a broadening of the peak at around 580 cm<sup>-1</sup> [27]. An apparent decrease on defects from the fresh to the post-reaction ZnO

NWs samples could be proposed. However, the presence of remaining adsorbed species, as evidenced from the *in-situ* DRIFTS-MS study, could contribute to some of the differences observed from XP, PL and Raman spectroscopy analysis of the post-reaction sample when compared to the fresh one.

For a deeper insight in the photocatalytic transformation of ethanol/water vapor over ZnO NWs, new separate *in-situ* DRIFTS-MS experiments were carried out over ZnO NWs and the reference ZnO thin film material. In these experiments, after ethanol/water vapor adsorption, the evolution of surface species under irradiation was followed by DRIFTS-MS. For such purposes, the sample was placed in the DRIFTS cell, purged under He flow and afterwards, flushed under dark conditions with the ethanol/water vapor; then, flushed with He until only He was detected by MS and then, light was switched on. Figure 6A and 6B show the corresponding spectra in the 1800-1300  $\text{cm}^{-1}$  region registered for ZnO NWs and ZnO thin film, respectively. After the ethanol/water vapor adsorption on ZnO NWs, Figure 6A, spectrum a, the observed bands can be attributed to adsorbed acetaldehyde, acyl, and different carboxylate and carbonate species, as discussed above. After three minutes of irradiation, the intensity of all the bands strongly decreased over the ZnO NWs sample (Figure 6A, spectrum b); meanwhile, besides acetaldehyde,  $\text{H}_2$ ,  $\text{CO}$ ,  $\text{CH}_4$  and  $\text{CO}_2$  were the products detected by on line MS analysis. On the other hand, several differences can be observed in the DRIFT spectrum after the ethanol/water vapor adsorption on ZnO thin film (Figure 6B, spectrum a). Less intense bands, related to adsorbed acetaldehyde and carboxylate and carbonate species, are obtained. Moreover, after illumination, only the band associated to adsorbed acetaldehyde

disappeared in this case (Figure 6B, spectrum b), and the main products detected were CO and CH<sub>4</sub> from the on line MS analysis; only minor amounts of CO<sub>2</sub> and H<sub>2</sub> were detected. These results indicate that the surface species generated after adsorption of ethanol/water vapor over ZnO NWs, are easily photo-transformed at room temperature, and contrarily, mainly irreversible carboxylate (and/or carbonate) species remains under irradiation on the reference ZnO film material.

## Conclusions

Crystalline ZnO nanowires prepared by a catalyst-free vapor-solid process were active in the photocatalytic hydrogen production from ethanol<sub>(aq)</sub> in gas phase. The surface species generated after adsorption of ethanol/water vapor over ZnO NWs, are easily photo-transformed at room temperature, and contrarily, mainly irreversible carboxylate (and/or carbonate) species remains under irradiation on a reference ZnO film. The photocatalytic behavior has been related with the 1D nanostructure characteristics of ZnO NWs. The combination of different techniques allowed us to identify the presence of different defects in the ZnO NWs such as oxygen vacancies, which are related with their performance.

After the *in-situ* DRIFTS-MS photocatalytic study carried out, we propose several processes that could take place over ZnO NWs during the irradiation in gas phase of an ethanol/water vapor flow at room temperature. The first step could be the photocatalytic transformation of ethanol into acetaldehyde and H<sub>2</sub>. Once acetaldehyde is formed, the photocatalytic transformation of acetaldehyde in the presence of water vapor could produce H<sub>2</sub> and acetic acid; acetaldehyde

also decomposes forming CO and CH<sub>4</sub> and acid acetic easily photo-transform to CO<sub>2</sub> over ZnO NWs.

The characteristics of ZnO NWs resulted almost unaltered after the photocatalytic process.

### **Conflicts of interest**

There are no conflicts to declare.

### **Acknowledgements**

The authors are grateful to MICINN-FEDER projects MAT2017-87500-P and PID2020-116031RBI00/AEI/10.13039/501100011033/FEDER for financial support and IREC and CCiTUB for characterization facilities. A.C.S. thanks the IREC for the PhD grant 06/10 and P.R.M-A. the ART2018 IN2UB project.

### **References**

[1] Di Mauro A, Cantarella M, Nicrota G, Privitera V, Impellizzeri G. Low temperature atomic layer deposition of ZnO: Applications in photocatalysis. Appl. Catal. B-Environ. 2016; 196:68-79.

<https://doi.org/10.1016/j.apcatb.2016.05.015>

[2] Pei Z, Ding L, Hu J, Weng S, Zheng Z, Huang M, Liu P. Defect and its dominance in ZnO films: A new insight into the role of defect over photocatalytic activity. Appl. Catal. B-Environ. 2013; 736-43.

<https://doi.org/10.1016/j.apcatb.2013.05.055>

- [3] Iglesias-Juez A, Viñes F, Lamiel-García O, Fernandez-García M, Illas F. Morphology effects in photoactive ZnO nanostructures: photooxidative activity of polar surfaces. *J. Mater. Chem, A*. 2015; 3:8782-92.  
<https://doi.org/10.1039/C5TA01111F>
- [4] Leelavathi A, Madras G, Ravishankar N. Origin of enhanced photocatalytic activity and photoconduction in high aspect ratio ZnO nanorods. *Phys. Chem. Chem. Phys.* 2013; 15:10795-802 <https://doi.org/10.1039/C3CP51058A>
- [5] Zhang X, Qin J, Xue Y, Yu P, Zhang B, Wang L, Liu R. Effect of aspect ratio and surface defects on the photocatalytic activity of ZnO nanorods. *Sci. Rep.* 2014; 4:4596 <https://doi.org/10.1038/srep04596>
- [6] Ye C, Bando Y, Shen G, Golberg D. Thickness-Dependent Photocatalytic Performance of ZnO Nanoplatelets. *J. Phys. Chem. B*. 2006; 110:15146-51.  
<https://doi.org/10.1021/jp061874w>
- [7] Han X-G, He H-Z, Kuang Q, Zhou X, Zhang X-H, Xu T, Xie Z-X, Zhen L-S. Controlling Morphologies and Tuning the Related Properties of Nano/Microstructured ZnO Crystallites. *J. Phys. Chem. C*. 2009; 113:584-9.  
<https://doi.org/10.1021/jp808233e>
- [8] Jang E S, Won J-H, Hwang S-J, Choy J-H. Fine Tuning of the Face Orientation of ZnO Crystals to Optimize Their Photocatalytic Activity. *Adv. Mater.* 2006; 18:3309-12. <https://doi.org/10.1002/adma.200601455>
- [9] Xu L, Hu Y-L, Pelligra C, Chen C-H, Jin L, Huang H, Sithambaram S, Aindow M, Joesten R, Suib S L. ZnO with Different Morphologies Synthesized by Solvothermal Methods for Enhanced Photocatalytic Activity. *Chem. Mater.* 2009; 21:2875-85. <https://doi.org/10.1021/cm900608d>



- [10] Mang A, Reimann K, Rübenacke St. Band gaps, crystal-field splitting, spin-orbit coupling, and exciton binding energies in ZnO under hydrostatic pressure. Sol. State Comm. 1995; 94:251-4. [https://doi.org/10.1016/0038-1098\(95\)00054-2](https://doi.org/10.1016/0038-1098(95)00054-2)
- [11] Ahmed F, Arshi N, Anwar M S, Danish R, Koo B H. Morphological evolution of ZnO nanostructures and their aspect ratio-induced enhancement in photocatalytic properties. RSC Advances. 2014; 4:29249-63. <https://doi.org/10.1039/C4RA02470B>
- [12] Pan H, Fen Y P. Semiconductor Nanowires and Nanotubes: Effects of Size and Surface-to-Volume Ratio. ACS Nano. 2008; 2:2410-14. <https://doi.org/10.1021/nn8004872>
- [13] Ong C B, Ng L Y, Mohammad A W. A review of ZnO nanoparticles as solar photocatalysts: Synthesis, mechanisms and applications. Renewable Sustainable Energy Rev. 2018; 81:536-51. <https://doi.org/10.1016/j.rser.2017.08.020>
- [14] Christoforidis K C, Fornasiero P. Photocatalytic Hydrogen Production: A Rift into the Future Energy Supply. ChemCatChem. 2017; 9:1523-44. <https://doi.org/10.1002/cctc.201601659>
- [15] Yao Y, Gao X, Li Z, Meng X. Photocatalytic Reforming for Hydrogen Evolution: A Review. Catalysts. 2020; 10:335. <https://doi.org/10.3390/catal10030335>
- [16] Kahng S, Yoo H, Km J H. Recent advances in earth-abundant photocatalyst materials for solar H<sub>2</sub> production. Adv. Powder Technol. 2020; 31:11-28. <https://doi.org/10.1016/j.apt.2019.08.035>

- [17] Güell F, Martínez-Alanis P R, Khachadorian S, Zamani R R, Franke A, Hoffmann A, Wagner M R, Santana G. Spatially controlled growth of highly crystalline ZnO nanowires by an inkjet-printing catalyst-free method. *Mat. Res. Exp.* 2016; 3:025010. <https://doi.org/10.1088/2053-1591/3/2/025010>
- [18] Xu X, Guo C, Qi Z, Liu H, Xu J, Shi C, Chong C, Huang W, Zhou Y, Xu C. Annealing effect for surface morphology and luminescence of ZnO film on silicon. *Chem. Phys. Lett.* 2002; 364:57-63. [https://doi.org/10.1016/S0009-2614\(02\)01281-2](https://doi.org/10.1016/S0009-2614(02)01281-2)
- [19] Khokhra R, Bharti B, Lee H N, Kumar R. Visible and UV photo-detection in ZnO nanostructured thin films via simple tuning of solution method. *Sci. Rep.* 2017; 7:15032. <https://doi.org/10.1038/s41598-017-15125-x>
- [20] Zhang X, Qin J, Xue Y, Yu P, Zhang B, Wang L, Liu R. Effect of aspect ratio and surface defects on the photocatalytic activity of ZnO nanorods. *Sci. Rep.* 2014; 4:4596. <https://doi.org/10.1038/srep04596>
- [21] Shchukarev A V, Korolkov D V. XPS Study of group IA carbonates. *Central European Journal Chemistry.* 2004; 2:347-62. <https://doi.org/10.2478/BF02475578>
- [22] Reparaz J S, Güell F, Wagner M R, Callsen G, Kirste R, Claramunt S, Morante J R, Hoffmann A. Recombination dynamics in ZnO nanowires: Surfaces states versus mode quality factor. *Appl. Phys. Lett.* 2010; 97:133116. <https://doi.org/10.1063/1.3496444>
- [23] Güell F, Osso J O, Goni A R, Cornet A, Morante J R. Direct imaging of the visible emission bands from individual ZnO nanowires by near-field optical spectroscopy. *Nanotech.* 2009; 20(31):315701. <https://doi.org/10.1088/0957-4484/20/31/315701>

- [24] Feng Y, Wang G, Liao J, Li W, Chen C, Li M, Li Z. Generation of convergent light beams by using surface plasmon locked Smith-Purcell radiation. *Sci. Rep.* 2017; 7;11622-1. <https://doi.org/10.1038/s41598-017-11622-1>
- [25] Zhan P, Wang W, Liu C, Hu Y, Li Z, Zhang Z, Zhang P, Wang B, Cao X. Oxygen vacancy–induced ferromagnetism in un-doped ZnO thin films. *J. Appl. Phys.* 2012; 111;003501. <https://doi.org/10.1063/1.3679560>
- [26] Djurisic A B, Leung Y H, Tam K H, Hsu Y F, Ding L, Ge W K, Zhong Y C, Wong K S, Chan W K, Tam H L, Cheah K W, Kwok W M, Philips D L. *Nanotech.* 2007; 18;095702. <https://doi.org/10.1088/0957-4484/18/9/095702>
- [27] Güell F, Martínez-Alanis P R, Khachadorian S, Rubio-Garcia J, Franke A, Hoffmann A, Santana G. Raman and photoluminescence properties of ZnO nanowires grown by a catalyst-free vapor-transport process using ZnO nanoparticle seeds. *Phys. Stat. Sol. B.* 2016; 253;883-88. <https://doi.org/10.1002/pssb.201552651>
- [28] Wu J J, Li S C. Catalyst-Free Growth and Characterization of ZnO Nanorods. *J. Phys. Chem. B.* 2002; 106;9546-51. <https://doi.org/10.1021/jp025969j>
- [29] Yee A, Morrison S J, Idriss H. A Study of the Reactions of Ethanol on CeO<sub>2</sub> and Pd/CeO<sub>2</sub> by Steady State Reactions, Temperature Programmed Desorption, and In Situ FT-IR. *J. Catal.* 1999; 186;279-95. <https://doi.org/10.1006/jcat.1999.2563>
- [30] Llorca J, Homs N, Ramírez de la Piscina P. In situ DRIFT-mass spectrometry study of the ethanol steam-reforming reaction over carbonyl-

derived Co/ZnO catalysts. *J. Catal.* 2004: 227;556-60.

<https://doi.org/10.1016/j.jcat.2004.08.024>

[31] Millar G J, Rochester C H, Waugh K C. Evidence for the adsorption of molecules at special sites located at copper/zinc oxide interfaces. Part 1.-A Fourier-transform infrared study of formic acid and formaldehyde adsorption on reduced and oxidised Cu/ZnO/SiO<sub>2</sub> catalysts. *J. Chem. Soc., Faraday Trans.* 1992: 88;1033-39. <https://doi.org/10.1039/FT9928801033>

[32] Millar G J, Rochester C H, Waugh K C. Evidence for the adsorption of molecules at special sites located at copper/zinc oxide interfaces. Part 2.-A Fourier-transform infrared spectroscopy study of methanol adsorption on reduced and oxidised Cu/ZnO/SiO<sub>2</sub> catalysts. *J. Chem. Soc., Faraday Trans.* 1992: 88;2257-61. <https://doi.org/10.1039/FT9928802257>

[33] Millar G J, Rochester C H, Waugh K C. Evidence for the adsorption of molecules at special sites located at copper/zinc oxide interfaces. Part 3.— Fourier-transform infrared study of methyl formate adsorption on reduced and oxidised Cu/ZnO/SiO<sub>2</sub> catalysts. *J. Chem. Soc., Faraday Trans.* 1992: 88;3497-503. <https://doi.org/10.1039/FT9928803497>

[34] Toyir J, Ramírez de la Piscina P, Homs N. Ga-promoted copper-based catalysts highly selective for methanol steam reforming to hydrogen; relation with the hydrogenation of CO<sub>2</sub> to methanol. *Int. J. Hydrogen Energy.* 2015: 40;11261-66. <https://doi.org/10.1016/j.ijhydene.2015.04.039>

[35] Ordonsky V V, Sushkevich V L, Ivanova I I. Study of acetaldehyde condensation chemistry over magnesia and zirconia supported on silica. *J. Mol. Catal. A.* 2010: 333;85-93. <https://doi.org/10.1016/j.molcata.2010.10.001>

- [36] Hauchecorne B, Terrens D, Verbruggen S, Martens J A, Van Langehove H, Demeestere K, Lenaerts S. Elucidating the photocatalytic degradation pathway of acetaldehyde: An FTIR in situ study under atmospheric conditions. , Appl. Catal. B Environ. 2011: 106;630-8. <https://doi.org/10.1016/j.apcatb.2011.06.026>
- [37] Carvalho D L, Borges L E P, Appel L G, Ramírez de la Piscina P, Homs N. In situ infrared spectroscopic study of the reaction pathway of the direct synthesis of n-butanol from ethanol over MgAl mixed-oxide catalysts. Catal. Today. 2013: 213;115-21. <https://doi.org/10.1016/j.cattod.2013.03.034>
- [38] Idriss H, Diagne C, Hindermann J P, Kiennemann A, Barteau M A. Reactions of Acetaldehyde on CeO<sub>2</sub> and CeO<sub>2</sub>-Supported Catalysts. J. Catal. 1995: 155;219-37. <https://doi.org/10.1006/jcat.1995.1205>
- [39] Rachmady W, Vannice M A. Acetic Acid Reduction by H<sub>2</sub> over Supported Pt Catalysts: A DRIFTS and TPD/TPR Study. J. Catal. 2002: 207;317-30. <https://doi.org/10.1006/jcat.2002.3556>
- [40] Sola A C, Homs N, Ramírez de la Piscina P. Photocatalytic H<sub>2</sub> production from ethanol(aq) solutions: The effect of intermediate products. Int. J. Hydrog. Energy. 2016: 41;19629-36. <https://doi.org/10.1016/j.ijhydene.2016.05.268>
- [41] Sola A C, Garzón-Sousa D, Araña J, González Díaz O, Doña Rodríguez J M, Ramírez de la Piscina P, Homs N. Differences in the vapour phase photocatalytic degradation of ammonia and ethanol in the presence of water as a function of TiO<sub>2</sub> characteristics and the presence of O<sub>2</sub>. Catal. Today. 2016: 266;53-61. <https://doi.org/10.1016/j.cattod.2015.08.008>
- [42] Sola A C, Ramírez de la Piscina P, Homs N. Behaviour of Pt/TiO<sub>2</sub> catalysts with different morphological and structural characteristics in the photocatalytic

conversion of ethanol aqueous solutions. *Catal. Today*. 2020: 341;13-20.

<https://doi.org/10.1016/j.cattod.2018.06.017>

[43] Llorca J, Ramírez de la Piscina P, Sales J, Homs N. Direct production of hydrogen from ethanolic aqueous solutions over oxide catalysts. *Chem. Comm.* 2001: 7;641-2. <https://doi.org/10.1039/B100334H>

[44] Güell F, Martínez-Alanis P R. Tailoring the Green, Yellow and Red defect emission bands in ZnO nanowires via the growth parameters. *J. Luminiscence*. 2019: 210;128-34. <https://doi.org/10.1016/j.jlumin.2019.02.017>

## Legend to the Figures

**Figure 1.** FESEM images of ZnO NWs: a) fresh; b) post-reaction.

**Figure 2.** A) XRD pattern of fresh ZnO NWs. In the inset, zoom of the ZnO (002) peak; B) TEM image of a ZnO NW visualized in the zone axis  $[-1100]$  and HRTEM micrograph of the marked zone; the inset shows the Fourier Transform image that corresponds to wurtzite ZnO.

**Figure 3.** O 1s core level spectra of ZnO NWs: a) fresh; b) post-reaction.

**Figure 4.** A) Room-temperature PL spectra of fresh and post-reaction NWs; B) Raman spectra of fresh and post-reaction ZnO NWs.

**Figure 5.** A) Mass spectra profiles of different products evolved during the irradiation at 28 °C of ZnO NWs under a He flow saturated with 1/9.6 (mol/mol) ethanol/water vapor; B) *in-situ* DRIFT spectra of ZnO NWs: a) under irradiation and a He flow saturated with 1/9.6 (mol/mol) ethanol/water vapor; b) after (a), light off and switch the reactants flow to He flow.

**Figure 6.** *In-situ* DRIFT spectra at 28 °C of: A) ZnO NWs, B) ZnO thin film; a) after adsorption in dark conditions of ethanol/water vapor (1/9.6 (mol/mol) ethanol/water) and flush with He; b) after (a), 3 min of irradiation.